Tight-binding analysis of coupling effects in metamaterials

Hao Xu, Qiong He, Shiyi Xiao, Bin Xi, Jiaming Hao, and Lei Zhou[a)]
State Key Laboratory of Surface Physics and Key Laboratory of Micro and Nano Photonic Structures (Ministry of Education), Fudan University, Shanghai 200433, China

(Received 20 October 2010; accepted 1 December 2010; published online 18 January 2011)

We established a generalized tight-binding method (TBM) to study the coupling effects in metamaterials. All parameters involved in our theory can be calculated from *first principles*, and the theory is applicable to general photonic systems with both dielectric and magnetic materials. As an illustration, we applied the theory to study the cutoff waveguides loaded with resonant electric/magnetic metamaterials. We not only accurately computed the coupling strengths between two resonant metamaterials, but also revealed a number of interesting coupling-induced phenomena. Microwave experiments and full-wave numerical simulations were performed to successfully verify all predictions drawn from the TBM. © *2011 American Institute of Physics*.
[doi:10.1063/1.3533948]

I. INTRODUCTION

Electromagnetic (EM) metamaterials are man-made composite materials composed by subwavelength resonant microstructures, which possess desired values of permittivity ε and permeability μ dictated by these microstructures. Because of their many potential applications, metamaterials have attracted extensive attention in recent years.[1–6] Lots of unusual properties have been discovered based on metamaterials, such as negative refraction,[1] superimaging and hyperimaging,[2,3] unusual EM wave tunneling,[4] optical magnetism,[5] polarization control,[6] and so on. Typically, these unusual effects were realized by metamaterials that can be homogenized as effective media, and the physical effects were well understood by the effective-medium theory (EMT) theoretically.

Recently, much attention was paid to the phenomena induced by mutual couplings between different elements in a metamaterial.[7–10] For example, a coupled multilayer fishnet structure exhibits completely different EM properties when one changes the interlayer distance very slightly;[7] a multilayer of split ring resonators with different orientations was found to exhibit very rich resonance spectra, dictated by the mutual couplings between adjacent layers;[8] the plasmonic modes in a metal nanoparticle chain exhibit completely different dispersion relations when stimulated by EM waves with different polarizations;[9] and the transmission/reflection/absorption spectrums of a double-stacking metamaterial structure depend sensitively on the lateral displacement between two layers.[10] Apparently, these intriguing phenomena can *not* be explained by the EMT.

Very recently, there appears another example induced by the coupling effects in metamaterials. It was found that an opaque cutoff waveguide becomes transparent for EM waves when loaded with electric/magnetic resonant metamaterials.[11–13] A simple EMT was developed to understand such unusual phenomena,[13] in which the waveguide is assumed as an electric (magnetic) plasma for transverse-electric (transverse-magnetic) wave, and inserting resonant structures modify the effective ε_{eff}, μ_{eff} of the entire system to make the cutoff waveguide transparent under certain conditions. While the EMT has explained most features of the experimental and simulation results,[11–13] there remain several features that can *not* be explained by the EMT. For example, although the EMT could reproduce the bandwidth of the transparency band quantitatively, it could not explain why there are a number of transmission peaks inside the transparency band and what determines the positions of these peaks.[13] Also, the EMT cannot tell us what happens if the inserted metamaterial layers are arranged nonperiodically. All these features are actually induced by the couplings between different resonant metamaterials inside the waveguide, and thus could not be explained by the simple EMT.

In viewing these previous works,[7–13] we find it highly desirable to develop an efficient theoretical approach to study the coupling effects in metamaterials. While full-wave numerical simulations can in principle yield all information of EM wave propagations in such systems,[7–13] the calculations are usually time consuming and the obtained results are not transparent enough to elucidate the inherent physics, particularly in complicated systems involving both electric and magnetic resonant materials.[8] Furthermore, sometimes such calculations even face difficulties to identify a particular eigenmode in complex systems, due to the "dark-mode" problem.[14] On the other hand, the tight-binding method (TBM), originally developed for electronic systems,[15,16] was recently extended to photonic systems.[17–22] The TBM seems to be a good approach to study the coupling effects in such systems. Unfortunately, so far the established TBM was only applicable to systems with nontrivial $\varepsilon(\vec{r})$ distribution, (e.g., photonic crystals),[17–23] not to metamaterial systems in which both $\varepsilon(\vec{r})$ and $\mu(\vec{r})$ can be nontrivial. More seriously, the hopping integrals in most previous TBM studies were set as *adjustable* parameters, fixed by fitting with full-wave numerical calculations.[17–20] Although some authors did derive some formulas to calculate the coupling strengths in photonic systems,[21,22] the formulas were obtained based on the master equation[24] rather than the original Maxwell equations.

[a)]Electronic mail: phzhou@fudan.edu.cn.

Such a simplification makes the calculations for hopping parameters rather difficult in complex structures, as we will explain in Sec. II. In addition, the developed theory[21–23] is still *not* applicable to metamaterial systems in which both $\varepsilon(\vec{r})$ and $\mu(\vec{r})$ are nontrivial.

In this paper, we establish a generalized TBM to study the coupling effects in photonic metamaterials. Distinct from previous TBM studies,[17–23] the present theory is based on the original Maxwell equations and all involved hopping parameters can be calculated from *first principles* without any fitting procedures. In addition, our theory is applicable to photonic systems where both *electric and magnetic* materials are present. While strictly speaking the theory established in this paper applies to nondispersive media only, we will show later that it can also be applied to metamaterials with weak frequency dispersions (e.g., not near their resonance frequencies). As an illustration, we apply the generalized TBM to study the coupling effects in one particular metamaterial system—a metallic waveguide loaded with resonant metamaterials.[11–13] We find that the TBM has explained many features that *cannot* be explained by the simple EMT,[13] both *qualitatively* and *quantitatively*. Microwave experiments and finite-difference-time-domain (FDTD) simulations are performed to verify all predictions drawn from the TBM.

The present paper is organized in the following way. We first develop the generalized TBM for metamaterial systems in Sec. II. Some benchmark results are then presented in Sec. III to demonstrate the validity of the theory, and a detailed comparison with previous TBM was given. In Sec. IV, we employ the TBM, together with microwave experiments and FDTD simulations, to systematically study the eigenmode properties of the loaded waveguide systems with metamaterial slabs arranged periodically and nonperiodically. Conclusions are summarized in Sec. V.

II. TIGHT-BINDING THEORY FOR PHOTONIC METAMATERIALS

We first establish the generalized TBM for photonic metamaterials. The TBM is originally developed to describe the electronic states in solid-state physics.[16] In analogy to the Schrödinger equation, Xu *et al.*[25] showed that the Maxwell equations can be rewritten in a similar form

$$\mathrm{i}\frac{\partial}{\partial t}|\phi\rangle = \hat{\mathbf{H}}|\phi\rangle, \tag{1}$$

where the Hamiltonian operator is given by

$$\hat{\mathbf{H}}(\vec{r}) = \begin{pmatrix} 0 & \frac{\mathrm{i}}{\varepsilon(\vec{r})}\nabla\times \\ -\frac{\mathrm{i}}{\mu(\vec{r})}\nabla\times & 0 \end{pmatrix} \tag{2}$$

and the wave function is $|\phi\rangle = \begin{pmatrix} \vec{E}(\vec{r},t) \\ \vec{H}(\vec{r},t) \end{pmatrix}$. Here $\vec{E}(\vec{r},t)$ and $\vec{H}(\vec{r},t)$ are the electric and magnetic fields, and $\varepsilon(\vec{r})$, $\mu(\vec{r})$ are the absolute permittivity and permeability distributions of the system. We assume the system to be isotropic for simplicity. If the inner product is defined as $\langle\phi_1|\phi_2\rangle = 1/2\int d\vec{r}^3(\varepsilon\vec{E}_1^*\cdot\vec{E}_2 + \mu\vec{H}_1^*\cdot\vec{H}_2)$, one can easily prove that the Hamiltonian $\hat{\mathbf{H}}$ is a hermitian operator.[25]

Consider a system with several identical scatterers embedded inside a background medium described by ε_b, μ_b, the Hamiltonian can be formally written as

$$\hat{\mathbf{H}} = \hat{\mathbf{H}}_0 + \sum_j \hat{V}_j, \tag{3}$$

where $\hat{\mathbf{H}}_0$ describes the background medium and $\hat{V}_j$ the jth scatterer, which depends on $\varepsilon(\vec{r})$, $\mu(\vec{r})$ of the scatterer. We consider the situation that there are a series of EM states trapped by one scatterer, with wave functions exponentially decaying as leaving the scatterers. This is similar to the electronic states of a single atom. Consider one such localized state with eigenvalue ω_0. Mathematically, there exists a Wannier function satisfying

$$(\hat{\mathbf{H}}_0 + \hat{V}_j)|\phi_j(\vec{r})\rangle = \omega_0|\phi_j(\vec{r})\rangle. \tag{4}$$

Such a Wannier wave function, highly localized around the jth scatterer, can be obtained by either solving Eq. (4) or the original Maxwell equations. Based on the tight-binding approximation[16] which is apparently valid in such a case, we can formally rewrite the overall Hamiltonian in a second quantization form as

$$\hat{\mathbf{H}} = \sum_j (\omega_0 + t_{j,j})a_j^\dagger a_j + \sum_{j\neq l} t_{j,l}a_j^\dagger a_l = \sum_{j,l} H_{j,l}a_j^\dagger a_l, \tag{5}$$

where $a_j^\dagger$ and a_j are the creation and annihilate operators of EM states at a point j, and the hopping parameters are defined as

$$\begin{aligned} t_{j,l} &= \langle\phi_j|\hat{\mathbf{H}} - (\hat{\mathbf{H}}_0 + \hat{V}_l)|\phi_l\rangle/\langle\phi_l\,|\phi_l\rangle \\ &= \langle\phi_j|\sum_{i\neq l}\hat{V}_i|\phi_l\rangle/\langle\phi_l\,|\phi_l\rangle. \end{aligned} \tag{6}$$

Here $|\phi_l\rangle$ is the wave function of the localized mode trapped by the lth scatterer. All eigenstates of the entire system can be obtained by diagonalizing the Hamiltonian matrix

$$H_{j,l} = (\omega_0 + t_{j,j})\delta_{j,l} + t_{j,l}. \tag{7}$$

In this paper, we neglect the onsite correction term $t_{j,j}$ which is very small, and only consider the hopping terms between nearest-neighbor (NN) and next-nearest-neighbor (NNN) pairs. The calculations can be significantly simplified for a system with translational invariance symmetry. In that case, applying a Fourier transformation to Eq. (5), we get

$$\hat{H} = \sum_{\vec{k}} \omega(\vec{k})a_{\vec{k}}^\dagger a_{\vec{k}}, \tag{8}$$

where $\omega(\vec{k})$ is the dispersion of the photonic band with $\vec{k}$ being the Bloch wave vector. For a one-dimensional system, we find that

$$\omega(k) = \omega_0 + 2t_{\mathrm{NN}}\cos(ka) + 2t_{\mathrm{NNN}}\cos(2ka). \tag{9}$$

Therefore, the EM wave properties of the entire system are known after the parameters ω_0, t_{NN}, and t_{NNN} are determined. Distinct from many previous TBM studies,[17–20] here all in-

volved parameters can be directly calculated from Eqs. (4) and (6), without any fitting procedures.

III. BENCHMARK TESTS ON DOUBLE-WELL MODELS

Before investigating realistic metamaterial systems, we first apply the theory to study some simple and solvable models as benchmark tests. The model systems that we consider are metallic waveguides with $b \times d$ rectangular cross sections, inserted with either dielectric slabs or magnetic slabs.

Consider the first case where the inserted slab is $2a$-thick with a permittivity ε_{in}, then the potential contributed by this scatterer (the dielectric slab) is found as

$$\hat{V} = \begin{cases} \begin{pmatrix} 0 & \mathrm{i}(\varepsilon_{\text{in}}^{-1} - \varepsilon_0^{-1}) \nabla \times \\ 0 & 0 \end{pmatrix}, & z \in [-a,a] \\ 0, & \text{elsewhere} \end{cases}, \tag{10}$$

where ε_0 is the absolute permittivity for vacuum (background medium). Suppose $b \geq d$ and consider the fundamental TE_{10} waveguide mode, we only need to explicitly study the E_y components since other field components can be derived similarly. At frequencies below cutoff, i.e., $\omega < \omega_c = c\pi/b$ with c the speed of light, the EM wave inside the waveguide is evanescent. Meanwhile, if ε_{in} is large enough so that $\omega_c^{\text{in}} = \sqrt{\varepsilon_0/\varepsilon_{\text{in}}} \times c\pi/b < \omega$ where ω_c^{in} is the cutoff frequency for the waveguide loaded with the dielectric, localized EM modes can be trapped in the dielectric slab located in $z \in [-a,a]$, with tails exponentially decaying to both sides of the dielectric slab. Therefore, the wave function of this trapped mode is

$$E_y \sim \begin{cases} \mathrm{e}^{\kappa z}, & z < -a \\ A\mathrm{e}^{\mathrm{i}kz} + B\mathrm{e}^{-\mathrm{i}kz}, & -a < z < a \\ \mathrm{e}^{-\kappa z}, & z > a \end{cases}, \tag{11}$$

where A and B are some parameters determined by matching boundary conditions. This is analogous to the trapped quantum well states in a quantum electronic system,[26] with the high-dielectric medium here behaving as a quantum well for photons. The concrete wave functions of the trapped states depend on the detailed model parameters, and can be easily calculated with a transfer-matrix-method (TMM),[27] slightly modified for such waveguide case.[28]

As an explicit example, we put a 5 mm-thick dielectric slab (with $\varepsilon_{\text{in}} = 10\varepsilon_0$) into a 50 mm-long waveguide with a 10 mm $\times$ 10 mm cross section, and calculate the transmission coefficient of TE_{10} mode through the waveguide. The calculated transmission spectrum is depicted in Fig. 1(a), from which a localized mode is easily identified at $f = 6.567$ GHz.[29] We will use f to denote the linear frequencies and ω to denote the circular frequencies throughout this paper. We then calculate the distribution of E_y at this frequency, and depict the field pattern in Fig. 1(b). The pattern shows clearly that this is a "quantum well" state for photons.

We now apply the TBM developed in Sec. II to study a "double-well" system—the same waveguide but loaded with two identical slabs. For such a system, the Hamiltonian can be written as the following matrix

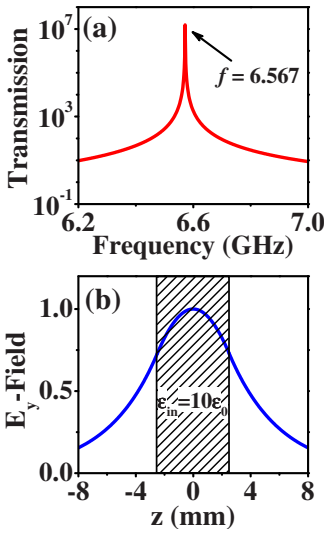

FIG. 1. (Color online) (a) TE_{10}-mode transmission spectrum through a 50 mm-long waveguide (with a 10×10 mm^2 cross section) loaded with a 5 mm-thick dielectric slab ($\varepsilon_{\text{in}} = 10\varepsilon_0$), calculated by the TMM, (b) field distribution of E_y calculated by the TMM at $f = 6.567$ GHz.

$$\hat{H} = \begin{pmatrix} \omega_0 & t_{\text{NN}} \\ t_{\text{NN}} & \omega_0 \end{pmatrix}. \tag{12}$$

Diagonalizing the Hamiltonian matrix (12), we found two eigenstates with eigen frequencies and wave functions given by

$$\omega = \begin{cases} \omega_0 + t_{\text{NN}}, & |\psi^+\rangle = |\phi_1\rangle + |\phi_2\rangle \\ \omega_0 - t_{\text{NN}}, & |\psi^-\rangle = |\phi_1\rangle - |\phi_2\rangle \end{cases}. \tag{13}$$

Let us first identify the sign of the hopping integral t_{NN}. We find from Eq. (6) that

$$\begin{aligned} t_{\text{NN}} &\approx \langle \phi_1 | \hat{V}_1 | \phi_2 \rangle / \langle \phi_1 \, | \phi_1 \rangle \\ &= \frac{1}{\langle \phi_1 \, | \phi_1 \rangle} \int_{\text{slab1}} d\vec{r}^3 [\varepsilon_{\text{in}} \vec{E}_1^*(\vec{r}), \vec{H}_1^*(\vec{r})] \\ &\quad \cdot \begin{bmatrix} 0 & \mathrm{i}\left[\frac{1}{\varepsilon_{\text{in}}(\vec{r})} - \frac{1}{\varepsilon_0}\right] \nabla \times \\ 0 & 0 \end{bmatrix} \begin{bmatrix} \vec{E}_2(\vec{r}) \\ \vec{H}_2(\vec{r}) \end{bmatrix} \end{aligned} \tag{14}$$

in which the integration is over the region where the slab 1 is located, and $\vec{E}_1(\vec{r})$, $\vec{E}_2(\vec{r})$ are the wave functions of the eigenmodes trapped by the two slabs. A straightforward calculation shows that

$$t_{\text{NN}} = \frac{1}{\langle \phi_1 \, | \phi_1 \rangle} (\varepsilon_0 - \varepsilon_{\text{in}}) \omega_0 \int_{\text{slab 1}} d\vec{r}^3 \vec{E}_1^* \cdot \vec{E}_2. \tag{15}$$

It is easy to prove that the normalization constant

$$\begin{aligned} \langle \phi_1 \, | \phi_1 \rangle = 2 &\int_{-\infty}^{-a/2} d\vec{r}^3 (\varepsilon_0 \vec{E}_1^* \cdot \vec{E}_1 + \mu_0 \vec{H}_1^* \cdot \vec{H}_1) \\ &+ \int_{-a/2}^{a/2} d\vec{r}^3 (\varepsilon_{\text{in}} \vec{E}_1^* \cdot \vec{E}_1 + \mu_0 \vec{H}_1^* \cdot \vec{H}_1), \end{aligned}$$

yields a *positive* value here. Noting that $\varepsilon_{\text{in}} \gg \varepsilon_0$ inside the slab and that $\vec{E}_1^* \cdot \vec{E}_2 > 0$ in slab 1 [see Fig. 1(b)], we identify

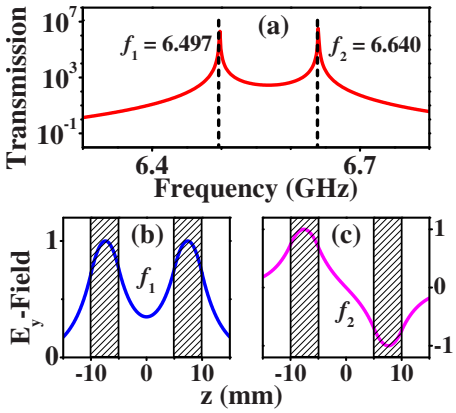

FIG. 2. (Color online) (a) TE_{10}-mode transmission spectrum through a 50 mm-long waveguide loaded with two dielectric slabs separated by a distance 15 mm, calculated by the TMM. Normalized field distributions of E_y calculated by the TMM at frequencies (b) f_1=6.497 GHz and (c) f_2 =6.640 GHz.

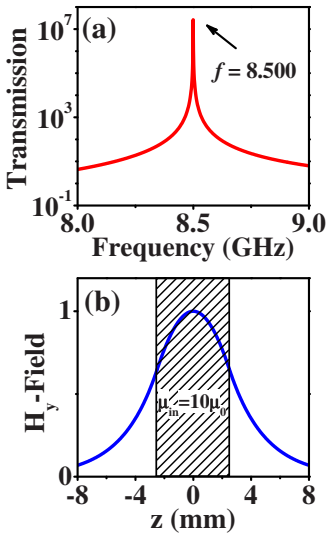

FIG. 3. (Color online) (a) TM_{11}-mode transmission spectrum through a 50 mm-long waveguide loaded with a 5 mm-thick magnetic slab ($\mu_{in}=10\mu_0$), calculated by the TMM, (b) Field distribution of H_y calculated by the TMM at f=8.500 GHz.

from Eq. (15) that the hopping integral is a *negative* value ($t_{NN}<0$). Therefore, Eq. (13) tells us that, for such a double-well system, the lower (higher) frequency mode exhibits an even (odd) symmetry.

We now determine the absolute value of t_{NN}, assuming that the two slabs are separated by a distance 15 mm. Put the calculated wave functions of a single mode [E_y component has been shown in Fig. 1(b)] and other necessary parameters into Eq. (15), we performed the integrations numerically. The calculated result is $t_{NN}=-0.071\times 2\pi$ GHz. Therefore, the TBM predicts that the two resonance modes for this double-well system should be at 6.496 GHz and 6.638 GHz (linear frequencies), respectively.

Numerical calculations are performed to verify the above TBM predictions. Figure 2(a) depicts the transmission spectrum for a waveguide loaded with two such slabs. Two eigenmodes with eigen frequencies f_1=6.497 GHz and f_2 =6.640 GHz are clearly identified in the spectrum,[29] whose positions are in excellent agreements with the TBM results labeled by two vertical lines. We further calculated the wave functions of these two eigenmodes, and illustrated the normalized E_y-field distributions in Figs. 2(b) and 2(c) for the lower and higher frequency modes, respectively. It is clearly shown that the lower frequency mode at f_1 exhibits an even symmetry (the $|\phi_1\rangle+|\phi_2\rangle$ type), and the higher frequency mode at f_2 exhibits an odd symmetry (the $|\phi_1\rangle-|\phi_2\rangle$ type), verifying the predictions of the TBM.

Distinct from previous TBMs which are limited to "*electric*" photonic systems,[17–23] the present TBM is much more general and can be applied to study "*magnetic*" photonic systems as well. As an illustration, we studied the TM_{11} mode transmission properties of the same waveguide but loaded with a 5 mm-thick magnetic slab (with $\mu_{in}=10\mu_0$). The calculated transmission spectrum is depicted in Fig. 3(a), where a localized mode is easily identified at f =8.500 GHz.[29] From the H_y field pattern depicted in Fig. 3(b) for this mode, we understand that this is again a "quantum well" state for photons, but contributed by the magnetic slab. Following the TBM, we find that the hopping integral is now determined by

$$t_{NN}=\frac{1}{\langle\phi_1\,|\phi_1\rangle}(\mu_0-\mu_{in})\omega_0\int_{\text{slab 1}} d\vec{r}^3\vec{H}_1^*\cdot\vec{H}_2, \tag{16}$$

with the normalization constant given by

$$\langle\phi_1\,|\phi_1\rangle=2\int_{-\infty}^{-a/2} d\vec{r}^3(\varepsilon_0\vec{E}_1^*\cdot\vec{E}_1+\mu_0\vec{H}_1^*\cdot\vec{H}_1)$$
$$+\int_{-a/2}^{a/2} d\vec{r}^3(\varepsilon_0\vec{E}_1^*\cdot\vec{E}_1+\mu_{in}\vec{H}_1^*\cdot\vec{H}_1).$$

Set the distance between two magnetic slabs as 15 mm, we performed numerical TMM calculations to find that $t_{NN}=-0.0194\times 2\pi$ GHz. Figure 4(a) depicts the TM_{11}-mode transmission spectrum through the waveguide but loaded with two such magnetic slabs separated by a distance of 15 mm. Similar to the electric case, two eigenmodes[29] are found at frequencies f_1=8.480 GHz and f_2=8.519 GHz in the spectrum, whose positions are in excellent agreements with

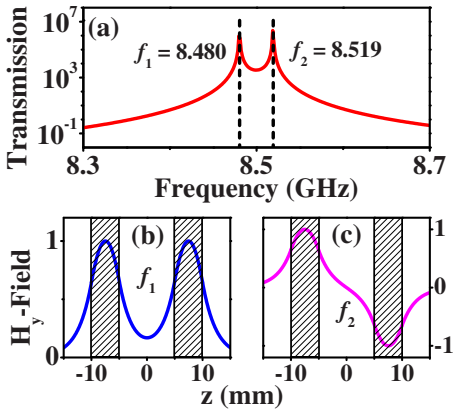

FIG. 4. (Color online) (a) TM_{11}-mode transmission spectrum through a 50 mm-long waveguide loaded with two magnetic slabs separated by a distance 15 mm, calculated by the TMM. Normalized field distributions of H_y calculated by the TMM at frequencies, (b) f_1=8.480 GHz and (c) f_2 =8.519 GHz.

the TBM results labeled by two vertical lines. We note that t_{NN} also takes a negative value here, similar to the previous electric case. Therefore, Eq. (13) tells us that the symmetries of the two eigenmodes are the same as those of the electric system. Indeed, the calculated wave functions of these two eigenmodes (Fig. 4) show that the lower (higher) frequency mode exhibits an even (odd) symmetry, again in perfect agreement with the TBM predictions [Eq. (13)].

The two benchmark tests presented above clearly illustrate the advantages of our theory as compared to previous versions of TBM.[17–23] Whereas the hopping parameters in most previous studies were set as adjustable parameters,[17–20] the present theory has provided a *first-principles* approach to determine these parameters. Although a TBM version[21,22] was previously available to compute the absolute values of the hopping parameters, that theory was limited to *electric* photonic systems. Furthermore, the hopping integral in that theory[22] can be written as

$$t_{NN} = \frac{c}{2\omega_0 \langle \vec{H}_2(\vec{r}) | \vec{H}_2(\vec{r}) \rangle} \int_{\text{scatter 1}} \vec{H}_1^*(\vec{r}) \cdot \nabla \left[\left(\frac{1}{\varepsilon_{in}(\vec{r})} - \frac{1}{\varepsilon_0} \right) \nabla \times \vec{H}_2(\vec{r}) \right] d\vec{r}^3, \quad (17)$$

which is much more complicated than our results. In particular, expanding Eq. (17), we find that there is *inevitably* a complicated *surface integral* over the interface between background medium and the scatterer [see Eq. (2.20) in Ref. 22], which comes from the term $\nabla[1/\varepsilon(r)]$ in Eq. (17). This is because the Hamiltonian adopted there[21,22] is derived from the master equation instead of the original Maxwell equations. In cases where $\varepsilon(r)$ is highly inhomogeneous and/or the scatterer/medium interface is complex, the calculations based on Eq. (17) are very difficult to handle. In contrast, our Hamiltonian is derived from the original Maxwell equations so that it does not contain such a troublesome $\nabla[1/\varepsilon(r)]$ term. As the results, the calculations for the hopping integrals are much easier to handle in our theory, particularly for structures with complex $\varepsilon_{in}(\vec{r})$ distributions and scatterer/medium interfaces. Finally, the present theoretical treatment differs sharply from many previous theories. For example, a plane-wave contribution is included to account for the background medium in Ref. 17, while it is subtracted from the scattering potential matrix in present approach.

IV. APPLICATIONS TO REALISTIC SYSTEMS

Encouraged by the promising benchmark results obtained on the double-well models, in this section, we apply the TBM to study the realistic systems—a WR90 waveguide [with a 22.86×10.16 mm^2 cross section, see Fig. 5(a)] loaded with multiple slabs of electric resonant metamaterials. The metamaterial that we designed is a metallic cross structure deposited on a dielectric substrate, with geometry shown in Fig. 5(a).

Following the TBM, we first calculate the properties of the eigenmode trapped by one scatterer. Put one electric metamaterial slab into the waveguide, we employ the FDTD method[30] to calculate the transmission spectrum through the

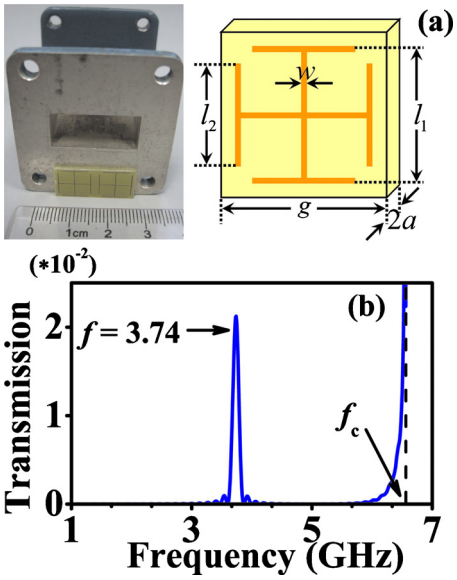

FIG. 5. (Color online) (a) (Left) A picture showing the WR90 waveguide and the electric resonant metamaterial adopted in our experiments; (right) geometry of the unit cell structure with parameters $g=11.43$ mm, $2a=1.2$ mm, $l_1=9$ mm, $l_2=7.4$ mm, $w=0.2$ mm. Here the dielectric constant of the substrate is 3.5, (b) TE_{10}-mode transmission spectrum through a 10 mm-long waveguide loaded with one metamaterial layer, calculated by FDTD simulations.

loaded waveguide under the TE_{10} mode excitation. The FDTD-calculated spectrum is depicted in Fig. 5(b), showing that there is indeed a localized mode trapped by the metamaterial slab with eigen frequency $f=3.74$ GHz, far below the waveguide cutoff frequency $f_c=6.56$ GHz denoted by a dashed line. FDTD simulations revealed that this trapped mode has similar eigenwave properties as that depicted in Fig. 1(b). However, the local EM field distribution is very complicated induced by the scatterings of the metallic elements, especially at the vicinities near the metamaterial structure. Such complicated local field distributions make it difficult to directly compute the hopping parameters employing the TBM established in Sec. II. More seriously, the singular behaviors of $\varepsilon(\vec{r})$ inside a metal further complicate the theoretical treatment established in Sec. II.

This problem can be solved with the concept of "metamaterials." We note that the realistic metamaterial slab [as shown in Fig. 5(a)] can be treated as a homogeneous 1.2 mm-thick effective-medium slab with relative dielectric constant given by $\varepsilon_r^{in}=1+(280/5.08^2-f^2)+(1950/15.95^2-f^2)$. To prove this point, we employ the FDTD method to calculate the transmission spectrum of normally incident plan waves through a realistic metamaterial slab (with microstructure periodically repeated), and compare the result with that calculated on the effective-medium slab. Good agreement is found between the two spectra, as seen from Fig. 6. The discrepancies near the resonance frequency are caused by standard Fabry–Perot interferences in the effective medium slab. We further employ the FDTD method to recalculate the TE_{10}-mode transmission spectrum for the same waveguide, but with the realistic metamaterial slab replaced by the effective-medium slab. The calculated spectrum shows that a resonance mode appears essentially at the same frequency.

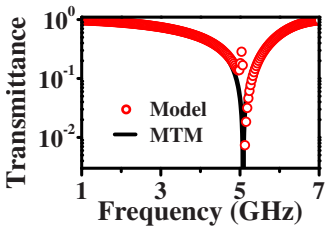

FIG. 6. (Color online) Normal-incidence plane-wave transmission spectra for a realistic metamaterial (MTM) slab and a homogeneous model slab with $\varepsilon_r^{in}=1+(280/5.08^2-f^2)+(1950/15.95^2-f^2)$, calculated by FDTD simulations.

These two facts have unambiguously demonstrated the validity to treat the complicated metamaterial slab by an effective-medium slab. Such a replacement greatly simplifies our calculations, and makes the calculations tractable. However, we note that the effective-medium slab possesses a frequency dependent permittivity, while the TBM developed in Sec. II only works for nondispersive medium in principle. Fortunately, when the interlayer distance is large enough so that the hopping integral is small, we expect that the frequency dispersion of the permittivity is not important, and therefore the present theory is still valid.

Treating the realistic structure as a homogeneous slab to obtain all information of the eigenmode trapped by a single slab, and assuming the distance between two adjacent slabs as 10 mm, we followed the approach as we did in Sec. III to calculate all the hopping parameters. The obtained TBM parameters are

$$\omega_0 = 3.74 \times 2\pi \text{ GHz}, \quad t_{NN} = -0.338 \times 2\pi \text{ GHz}, \quad t_{NNN} = -0.08 \times 2\pi \text{ GHz}. \tag{18}$$

We emphasize that this set of parameters are obtained from *direct* calculations based on our theory, *without using any adjustable parameters*.[17–20] Using this set of parameters, we can employ the TBM to calculate the eigenmode properties in those systems with *arbitrary* number of slabs. Given a particular configuration, we can diagonalize the corresponding Hamiltonian matrix to get not only all the eigenmode frequencies, but also the EM wave distributions for each mode. While full-wave numerical simulations can yield similar information, the TBM calculation is much simpler, and can provide much more physical insights. In particular, we will show later that the TBM can help us identify some eigenmodes with very weak strengths, which are difficult to detect in FDTD simulations.

We employed the TBM to calculate the eigenmodes in the waveguides loaded with 2, 3, 4, and 5 layers. The calculated eigenmode frequencies (linear frequencies) are labeled by solid lines in the right panels of Figs. 7(a)–7(d), correspondingly. For a system with N inserting slabs, the Hamiltonian matrix is $N \times N$ yielding N eigen frequencies, as shown in Fig. 7. To validate the TBM, we performed microwave experiments and FDTD simulations[30] to study the transmission spectra through the WR90 waveguides loaded with 2, 3, 4, and 5 metamaterial slabs (keeping the interlayer distance as 10 mm). In our experiments, we used a 5 mm-long monopole antenna to excite the TE_{10} mode at the front side of the loaded waveguide, and employed another identical antenna to measure the signals transmitted through the waveguides. The experimental setup is basically the same as that in Ref. 13 (see Fig. 1 in Ref. 13). The experimental and FDTD simulation results are shown in the left and middle panels of Figs. 7(a)–7(d), for waveguides with 2, 3, 4, and 5 metamaterials slabs, correspondingly. First, we note that the FDTD results are generally in good agreements with the experimental spectra. More importantly, we note that the positions of those transmission peaks (both in FDTD and in experiments) are in rather satisfactory agreements with the eigen frequencies predicted by the TBM. In particular, we note that some eigenmodes [say, the highest mode in Figs. 7(c) and 7(d)] possess relatively weak couplings with external fields so that they are not easy to identify from experiments. In such cases, the TBM is particularly helpful to pick up those "dark" eigenmodes.

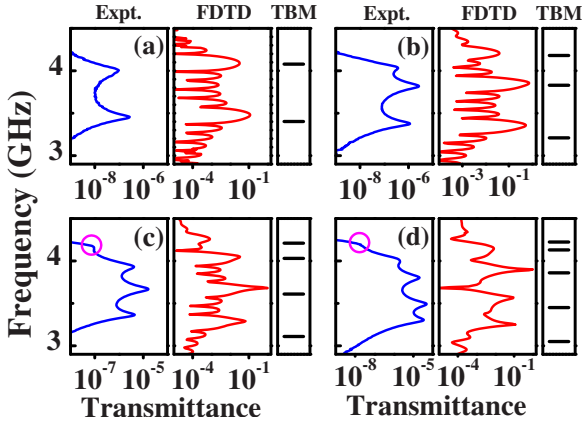

FIG. 7. (Color online) Experimental (left) and FDTD (middle) results of the transmission spectrum for the waveguides loaded with (a) 2, (b) 3, (c) 4, and (d) 5 metamaterial slabs. Right panels depict the positions of the eigenmodes predicted by the TBM.

The TBM can also be applied to study the system with infinite numbers of metamaterial slabs arranged periodically. For such a periodic system, the eigenmodes inside the system form an energy band, with dispersion relation given by Eq. (9). Putting the TBM parameters of Eq. (18) into Eq. (9), we calculated the dispersion relation and depicted the spectrum in Fig. 8 as open circles. Again, we performed numerical calculations to verify the TBM predictions. Treating the realistic metallic structures as homogeneous metamaterial slabs, we employed the TMM (Ref. 28) to calculate the EM wave dispersion relation, and drew the results in Fig. 8 as

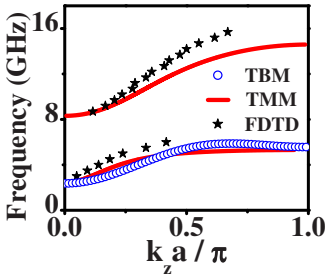

FIG. 8. (Color online) EM wave dispersion relations inside the loaded waveguides calculated by three different methods.

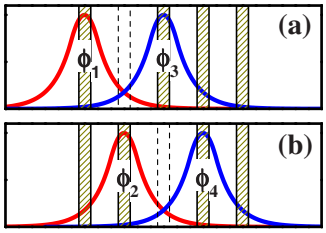

FIG. 9. (Color online) Geometries of two studied waveguides loaded with 4 metamaterial slabs arranged nonperiodically. Solid curves schematically show the wave functions of the eigenmodes trapped by particular slabs.

solid lines. We then employed the FDTD simulations[30] to compute the EM wave dispersion relation of the system with all microstructures fully taken into account. The FDTD-calculated dispersions are depicted as solid stars in Fig. 8. We can easily identify the upper branch as the waveguide mode with a cutoff frequency at 6.56 GHz. For this branch, we do not have the TBM results because the tight-binding approximation is no longer valid. On the other hand, the lower branch in the waveguide cutoff region is responsible for the anomalous high transmissions in the loaded waveguides.[11–13] For this branch, we find that the dispersion relations computed by the TMM and FDTD simulations are in good agreements with the TBM results. Such good agreements reinforced the notion that the TBM works quite well for such metamaterial systems.

In addition, the TBM developed in this paper can be employed to study the systems with slabs arranged *not periodically*. In what follows, we study two waveguide systems with 4 inserting slabs, obtained by removing one particular slab from a 5-slab periodic system. Such systems are relatively easy to study since we do not need to introduce additional TBM parameters, although the TBM developed here is not limited to such cases. In the first system as schematically shown in Fig. 9(a), we assume that the second slab is removed from the 5-slab system. We find that the Hamiltonian matrix is written as

$$\hat{H}' = \begin{pmatrix} \omega_0 & \frac{1}{2}t_{\mathrm{NNN}} & 0 & 0 \\ \frac{1}{2}t_{\mathrm{NNN}} & \omega_0 & t_{\mathrm{NN}} & t_{\mathrm{NNN}} \\ 0 & t_{\mathrm{NN}} & \omega_0 & t_{\mathrm{NN}} \\ 0 & t_{\mathrm{NNN}} & t_{\mathrm{NN}} & \omega_0 \end{pmatrix}. \tag{19}$$

It is worth noting that the matrix element $H'_{1,2}$ describing the hopping between the first and third slabs is not t_{NNN}, but acquires a factor of 1/2. The physics can be understood from the following argument. From Eq. (6), we understand that the dominant contributions to the NNN hopping term should be $t_{\mathrm{NNN}}=\langle\phi_1|\Sigma_{i\neq l}\hat{V}_i|\phi_3\rangle/\langle\phi_3\ |\phi_3\rangle \approx \langle\phi_1|\hat{V}_1+\hat{V}_2|\phi_3\rangle/\langle\phi_3\ |\phi_3\rangle$. If we remove the second slab (i.e., $\hat{V}_2=0$), the hopping between the first and third slabs becomes $\sim\langle\phi_1|\hat{V}_1|\phi_3\rangle/\langle\phi_3\ |\phi_3\rangle$. As seen from Fig. 9(a), to the lowest-order approximation, the product of two wave functions $\phi_1\cdot\phi_3$ yields almost the same value in regions occupied by slab 1 and slab 2 (which is vacant here). Therefore, we have approximately $\langle\phi_1|\hat{V}_1|\phi_3\rangle \approx \langle\phi_1|\hat{V}_2|\phi_3\rangle \approx (1/2)\langle\phi_1|\hat{V}_1+\hat{V}_2|\phi_3\rangle$, and in turn, $H'_{1,2} \approx (1/2)t_{\mathrm{NNN}}$. We note that this argument holds for all tight-binding systems, including both photonic and electronic ones. Diagonalizing this Hamiltonian matrix (19), we find four eigen (linear) frequencies, and label their positions as solid lines in the right panel of Fig. 10(a).

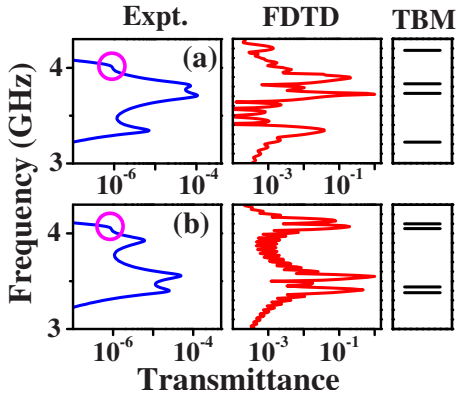

FIG. 10. (Color online) Experimental (left) and FDTD (middle) results of the transmission spectrum for the waveguides loaded with 4 metamaterial slabs, arranged following the geometries depicted in Fig. 9. Right panels depict the positions of the eigenmodes predicted by the TBM.

If the removed slab is the third one as shown in Fig. 9(b), the Hamiltonian matrix is found as

$$\hat{H}'' = \begin{pmatrix} \omega_0 & t_{\mathrm{NN}} & 0 & 0 \\ t_{\mathrm{NN}} & \omega_0 & \frac{1}{2}t_{\mathrm{NNN}} & 0 \\ 0 & \frac{1}{2}t_{\mathrm{NNN}} & \omega_0 & t_{\mathrm{NN}} \\ 0 & 0 & t_{\mathrm{NN}} & \omega_0 \end{pmatrix}. \tag{20}$$

Based on the same argument, we found that the hopping integral between the second and fourth slabs is $(1/2)t_{\mathrm{NNN}}$ instead of t_{NNN}. Again, the eigen (linear) frequencies obtained by diagonalizing the above matrix are depicted in the right panel of Fig. 10(b) as solid lines.

As shown in Fig. 10, the mode structures for these two systems are quite different although they both contain four slabs. For example, the middle two states are approaching each other in case 1, but in case 2, states 1 and 2 are approaching each other. These are caused by the modified effective hopping between adjacent layers, as already shown in Eqs. (19) and (20). Again, microwave experiments and FDTD calculations were performed to study the transmission spectra for these two particular systems. As shown in Fig. 10, the measured and the calculated spectra, which are in reasonable agreements with each other, show that the transmission speaks are in reasonable agreements with the TBM predictions. In particular, both experiments and FDTD simulations reproduced the mode structures predicted by the TBM, which demonstrates again the validity of the TBM in such systems.

We note that some discrepancies nevertheless exist between the TBM and FDTD/experimental results, particularly in multilayer systems (see Figs. 7 and 10). Such discrepancies are possibly caused by the omission of frequency dis-

persion in the present theory. Another possible reason is that the effective parameters obtained based on a single slab may change slightly when we study a multilayer system.

V. CONCLUSIONS

To summarize, we have established a generalized TBM to study the coupling effects in photonic metamaterials. The advantages of our theory are that it can determine all involved parameters from first principles, and can be applied to *general* photonic systems with both dielectric and magnetic materials. Taking the cutoff waveguides loaded with resonant metamaterials as explicit examples, we applied the TBM to study various interesting phenomena induced by the coupling effects in metamaterials. Our results showed that the TBM can provide not only quantitative measures on the coupling strengths between different resonant units, but also other information such as the symmetries of the eigenmodes, the resonant peak positions and the dispersion relations in periodic and even nonperiodic systems. Microwave experiments and FDTD simulations on realistic systems were performed to verify all the predictions drawn from the TBM. We believe that the present TBM, with some further developments to take the materials' frequency dispersions into account, can be employed to study many other metamaterial systems in which the coupling between different resonant units play important roles.

ACKNOWLEDGMENTS

This work was supported by the National Natural Science Foundation of China (Grant Nos. 60725417 and 60990321), and Shanghai Science and Technology Committee (Grant No. 08dj1400302).

[1]D. R. Smith, W. J. Padilla, D. C. Vier, S. C. Nemat Nasser, and S. Schultz, Phys. Rev. Lett. **84**, 4184 (2000).
[2]J. B. Pendry, Phys. Rev. Lett. **85**, 3966 (2000); N. Fang, H. Lee, C. Sun, and X. Zhang, Science **308**, 534 (2005).
[3]Z. Liu, H. Lee, Y. Xiong, C. Sun, and X. Zhang, Science **315**, 1686 (2007).
[4]M. Silveirinha and N. Engheta, Phys. Rev. Lett. **97**, 157403 (2006).
[5]N. Liu, H. Guo, L. Fu, S. Kaiser, H. Schweizer, and H. Giessen, Nature Mater. **7**, 31 (2008).
[6]J. M. Hao, Y. Yuan, L. X. Ran, T. Jiang, J. A. Kong, C. T. Chan, and L. Zhou, Phys. Rev. Lett. **99**, 063908 (2007).
[7]J. F. Zhou, T. Koschny, M. Kafesaki, and C. M. Soukoulis, Phys. Rev. B **80**, 035109 (2009).
[8]N. Liu, H. Liu, S. Zhu, and H. Giessen, Nat. Photonics **3**, 157 (2009).
[9]K. H. Fung and C. T. Chan, Opt. Lett. **32**, 973 (2007).
[10]N. Liu, L. Langguth, T. Weiss, J. Kästel, M. Fleischhauer, T. Pfau, and H. Giessen, Nature Mater. **8**, 758 (2009).
[11]R. Marqués, J. Martel, F. Mesa, and F. Medina, Phys. Rev. Lett. **89**, 183901 (2002).
[12]J. Esteban, C. Camacho-Peñalosa, J. E. Page, T. M. Martín-Guerrero, and E. Márquez-Segura, IEEE Trans. Microwave Theory Tech. **53**, 1506 (2005).
[13]H. Xu, Z. Y. Wang, J. M. Hao, J. J. Dai, L. X. Ran, J. A. Kong, and L. Zhou, Appl. Phys. Lett. **92**, 041122 (2008).
[14]M. W. Chu, V. Myroshnychenko, C. H. Chen, J. P. Deng, C. Y. Mou, and F. J. G. de Abajo, Nano Lett. **9**, 399 (2009).
[15]R. S. Mulliken, J. Chem. Phys. **23**, 1833 (1955).
[16]C. Kittle, *Introduction to Solid State Physics*, 5th ed. (Wiley, New York, 1976).
[17]E. Lidorikis, M. M. Sigalas, E. N. Economou, and C. M. Soukoulis, Phys. Rev. Lett. **81**, 1405 (1998).
[18]M. Bayindir, B. Temelkuran, and E. Ozbay, Phys. Rev. Lett. **84**, 2140 (2000).
[19]Y. Hara, T. Mukaiyama, K. Takeda, and M. Kuwata-Gonokami, Phys. Rev. Lett. **94**, 203905 (2005).
[20]M. Notomi, E. Kuramochi, and T. Tanabe, Nat. Photonics **2**, 741 (2008).
[21]D. Leuenberger, R. Ferrini, and R. Houdre, J. Appl. Phys. **95**, 806 (2004).
[22]A. Boag and B. Z. Steinberg, J. Opt. Soc. Am. A **18**, 2799 (2001).
[23]K. Busch, S. F. Mingaleev, A. Garcia-Martin, M. Schillinger, and D. Hermann, J. Phys.: Condens. Matter **15**, R1233 (2003).
[24]J. D. Joannopoulos, R. D. Maede, and J. N. Winn, *Photonic Crystals: Molding the Flow of Light*, 2nd ed. (Princeton University, Princeton, NJ, 1995).
[25]Y. Xu, Y. Li, R. K. Lee, and A. Yariv, Phys. Rev. E **62**, 7389 (2000).
[26]L. D. Landau and E. M. Lifshitz, *Quantum Mechanics: Non-Relativistic Theory*, 3rd ed. (Butterworth-Heinema, London, 1981).
[27]See, e.g., K. Busch, C. T. Chan, and C. M. Soukoulis, in *Photonic Band Gap Materials*, edited by C. M. Soukoulis (Kluwer, Dordrecht, 1996).
[28]For wave propagations in metallic waveguides (with cross section $a \times b$) loaded with multiple layers of homogeneous slabs, the TMM is essentially the same as that for the free-space cases (Refexcept that appropriate boundary conditions should be imposed for a particular waveguide mode. For example, for the TE_{10}-mode considered in the present paper, we need to fix $\vec{k}_{\parallel}=\hat{x}\pi/a$ in each layer (k_z can be calculated accordingly) and match the E_y and H_x at the boundaries between two layers. Similar techniques can be applied to study other waveguide modes.
[29]The response (i.e., transmittance and reflectance) should diverge when the system is stimulated at its eigenmode frequency. Here we add a tiny loss to make the transmittance still finite for the purpose of better illustration.
[30]CONCERTO 7.0, Vector Field Limited, England, 2008. A basic mesh sized 0.2 mm $\times$ 0.2 mm $\times$ 0.5 mm was adopted to discretize the realistic structures, and finer meshes were adopted wherever necessary. Convergences were carefully tested in our simulations. Appropriate Bloch boundary conditions were imposed at the boundaries between two unit cells in the calculations for the band structure.